Ultrasonics Sonochemistry 92 (2023) 106247

Contents lists available at ScienceDirect

Ultrasonics Sonochemistry

journal homepage: www.elsevier.com/locate/ultson

Sonochemical fabrication of gradient antibacterial materials based on Cu-Zn alloy

Mirna Sabbouh [a,1], Anna Nikitina [a,1], Elizaveta Rogacheva [b], Anna Nebalueva [a], Vladimir Shilovskikh [a,c], Roman Sadovnichii [a], Aleksandra Koroleva [c], Konstantin Nikolaev [a], Lyudmila Kraeva [b], Sviatlana Ulasevich [a,*], Ekaterina Skorb [a]

[a] ITMO University, 9 Lomonosova Street, 191002 St. Petersburg, Russia
[b] Pasteur Institute of Epidemiology and Microbiology, 14 Mira Street, Saint Petersburg 197101, Russia
[c] Saint-Petersburg State University, Russia

ARTICLE INFO

Keywords:
Ultrasonic treatment
Sonochemistry
Nanostructuring
Metal particles
Oscillations
Antibacterial properties

ABSTRACT

At present research, we highlight ultrasonic treatment as a new way to create materials with a gradient change of chemical or physical properties. We demonstrate the possibility to fabricate novel materials with biocide activity based on simple and cheap Cu-Zn alloy. In this research, we propose a green preparative technique for the sonication of an alloy in an alkali solution. The method leads to a significant visual change and differentiation of particles into three different fractions. Due to the chemical micro gradients in media near the solid surface under intensive sonication, fast formation of specific functional groups occurs on the particles' surface. The particles were studied X-ray diffraction analysis (XRD) analysis, the field-emission scanning electron microscope (SEM) as well as electron backscatter diffraction (EBSD) mode, X-ray Photoelectron Spectroscopy (XPS), the differential pulse anodic stripping voltammetry (DPASV) technique. A strong correlation of both methods proves a redistribution of copper ions from Fraction I to Fraction III that influence for the antibacterial properties of the prepared material. The different biocidal activity was demonstrated for each separated Fraction that could be related to their different phase content and ability to release the different types of ions.

1. Introduction

Ultrasound treatment finds application in medicine for drug delivery [1,2], in the medium and large-capacity industry [3–5], as fuel cell electrocatalysis [6–9], or green chemistry [10–12]. With the cavitation effect, sonochemically modification allows the formation of morphology changes on the surface. Ultrasound treatment of Al-Ni alloy was studied by Cherepanov et al. [6]. They reported fundamental relation between the cavitation effect and redox processes on the surface and surface composition, such as surface area and grain size. The ultrasound is also known to influence on the phase structure, grain sizes, and various defects [7]. Sonochemical treatment leads to significant particle transformation and several fraction formations [13]. The aluminium metallic particles are known to split after sonication, into three fractions: over-oxidized samples, monodisperse porous metal particles with a thin oxide layer, and unmodified ones. Phases were easily separated with sedimentation. Obtained fractions had different specific gravity and thus spontaneously differentiated into three phases. This approach is very perspective for studying the antibacterial properties [10,22]. In a recent paper [10], sonication was proposed to help to reveal the main mechanism of the antibacterial action of the studied materials, but can also be used to obtain antibacterial materials. Besides, the fraction separation helps to reveal the toxicity of each component [22].

Despite, Cu-Zn alloys are well-studied as a high-effective catalyst [14–16] and as a perspective material for biomedical applications the mechanisms of antibacterial properties are still being studied [13,17–19]. Experimental trials of brass and copper surfaces consistently report inhibition of bacterial growth but, evidence is still sparse as to a significant impact on hospital-acquired infections [20].

In this regard, the aim of our research is the development of the method for fabrication of the materials with enhanced antibacterial activity and study their antibacterial properties. For these purposes,

* Corresponding author.
E-mail address: saulasevich@itmo.ru (S. Ulasevich).
[1] Authors with equal contribution.

https://doi.org/10.1016/j.ultsonch.2022.106247
Received 5 April 2022; Received in revised form 20 November 2022; Accepted 25 November 2022
Available online 5 December 2022
1350-4177/© 2022 Published by Elsevier B.V. This is an open access article under the CC BY-NC-ND license (http://creativecommons.org/licenses/by-nc-nd/4.0/).

ultrasound treatment will be used. It is known that ultrasonic treatment makes it possible to obtain porous oxide layers based on which various functional surfaces can be created. In particular, the subsequent modification of such surfaces with pH-sensitive polyelectrolytes makes it possible to use the metabolism of bacteria to protect biocompatible surfaces was studied [21].

In our previous paper [22], we have found a unique synergy antibacterial effect of Zn^{2+} and Cu^{2+} ions against *St. aures* was revealed after the sonochemical treatment of brass particles [22]. Thus, we are planning to extend the research of ultrasonically prepared Cu-Zn biocide materials and estimate individual isolated fractions' activity. We will determine the effect of different ion-containing structures on the surface of the ultrasonically modified Cu-Zn alloy on bacterial strains and find out the role of released copper and zinc ions on bacteria growth.

2. Experimental section

Reagents. Sodium hydroxide (NaOH, ≥95 %), mercury nitrate ($Hg(NO_3)_2{\cdot}H_2O$, ≥98.5 %), nitric acid (HNO_3, 65.0–67.0 %), hydrochloric acid (HCl, 37 %), copper-zinc alloy (Cu-Zn alloy powder, 70 wt% copper, 30 wt% zinc, 60 mesh, CAS Number:63338–02-3) were purchased from Sigma Co ltd (USA). Distilled water used in the experiment is deionized water (18.2 mΩ).

Preparation of Cu-Zn Fractions. 5 g of Cu-Zn alloy were immersed in 100 mL of 0.5 M NaOH. The solution was sonicated using ultrasonic processor UIP1000hd (Hielscher Ultrasonics, Germany) for 30 min at the intensity of 87 W/cm^2. The apparatus was equipped with the titanium sonotrode BS4d408 with a head area of 12.5 cm^2. The maximal amplitude was 37 μm.

The sonochemical treatment of the particles was carried out using constant flow cooling system and temperature control. The coolant supply rate was regulated so that the temperature of cooled solution did not exceed + 45 °C. For more efficient cooling, a commercial liquid antifreeze was used in the flow cooling system. When we need to increase the cooling power, a mixture at a temperature of –55 °C based on ice and calcium chloride (hexahydrate crystalline) was used instead of liquid antifreeze. When the electrolyte temperature reached a plateau, the sonication was stopped, and the solution was cooled with a new cooling mixture. Thus, the average temperature of the bulk electrolyte was in a range of + 20 ÷ +45 °C.

If the experiment temperature rose above + 45 °C, then we repeated the experiment. After the treatment, the Cu-Zn particles were separated into three fractions by centrifugation at 1300 g for 5 min. The Fractions (I–III) were washed up with distilled water and dried at 120 °C for 24 h.

Sample characterization. The structural and morphological characterization of prepared Cu-Zn alloy samples was performed using the field-emission scanning electron microscope (SEM) Tescan Vega3 (TESCAN ORSAY HOLDING, Czech Republic). The electron backscatter diffraction (EBSD) images are acquired using Hitachi S-3400 N scanning electron microscope (SPBU, "Geomodel") equipped by backscattered electrons imaging mode. The sample were previously spattered with a carbon coating of 1 nm. The accelerating voltage was 20 kV. Cell cultures were studied with Hitachi S3400-N SEM at low acceleration voltage (5 kV).

X-ray Photoelectron Spectroscopy (XPS) spectra were acquired with a SPECS hemispherical energy analyzer (Phoibus 100) and SPECS focus 500 X-ray monochromator.

The X-ray diffraction analysis (XRD) analysis was performed by a D2 PHASER (Bruker, Germany) using Ni-filtered CuKα radiation (λ = 1.5418 Å). The sample powders were scanned in a 2θ range of 10-100° with a 0.02° step interval. The DIFFRAC.EVA integrated into Bruker's diffractometer D2Phaser was used to match different diffraction patterns to identify the contents of the samples. Quantitative phase analysis was performed utilising the algorithm implemented in TOPAS (Bruker, Germany).

Potentiometric titration. The differential pulse anodic stripping voltammetry (DPASV) technique was used for zinc and copper ions detection in samples of modified brass particles. For this purpose, the three-electrode system consisting of a working scan-printed electrode, a reference-based Ag/AgCl electrode, a platinum counter electrode (CE) was used. An electrochemical cell volume of 1 mL was used. The background electrolyte was prepared using mercury nitrate of 0.15 mM, 1.5 mM HNO_3, 0.05 M HCl. All electroanalytical measurements were repeated at least three times for the statistical evaluation of the results.

Antibacterial activity. The biological study was carried out on the most common pathogens of septic and nosocomial infections: *Staphylococcus aureus, Escherichia coli, Klebsiella pneumonia, Pseudomonas aeruginosa,* and *Enterobacter cloacae,* which are most often resistant to antibiotics. The selected strains were obtained from Culture Collection of the Saint-Petersburg Pasteur Institute (Saint-Petersburg, Russian Federation). Prior to each bacterial experiment, bacterial cultures were refreshed on nutrient agar (Dia-M, Russia). Fresh bacterial suspensions were grown overnight at 37 °C in nutrient broth, and bacteria were collected at the logarithmic stage of growth and the suspensions were adjusted to OD600 ¼ 0.3. The antimicrobial activity test was used to determine the biocide activity of modified Cu-Zn alloy particles. 5 μL of particle's solution at concentrations of 1 mg/mL was added to the grown lawn and incubated 24 h at 37 °C. After the inhibition zone was fixed. The samples were mounted and carbon-coated in preparation for scanning electron microscopy (SEM) imaging.

All experiments were reproduced at least three times using three samples of each group. Obtained data were averaged with the standard error of the mean. Statistical analysis was performed using ANOVA ($^*p < 0.05$).

3. Results and discussion

Currently, the development of biocidal materials for hospitals and self-cleaning surfaces is very relevant. We assume that to create a good antibacterial material, it is necessary to know the mechanism of its action. In our previous research [22], we have found a unique effect of the synenergetic action of zinc and copper ions. However, the antibacterial activity of combination of metal oxides not always provide the synergetic effect. [23] That is why it is important to study this effect.

The brass is chosen as a material for sonochemical modification because its biocidal properties is well-known and brass oxidation is well studied. That is why we are focused on study its sonochemical oxidation in a solution. We are interested in evaluating the difference between the two oxidation methods, as well as identifying the features of the antibacterial effect of fabricated phases.

We used an ultrasonic treatment in a 0.5 M sodium base for the experiment to form the functional groups on the surface. Ultrasound of high intensity is known to provide fast physical and chemical surface modification due to high energy generated by a sonotrode at a particular surface area [20]. This energy leads to the formation of cavitation bubbles that explosion creates the high-temperatures (up to 5000 K) and high-pressure values (up to 500 atm) [6–8]. It is a favorable environment for oxidative reactions to take place.

We assume the formation of an oxide and hydroxide films on the surface of brass particles under these conditions (Fig. 1 **a**). Our assumption could be confirmed by the fact that ultrasonic treatment leads to the formation of three fractions with different colors: Fraction I (yellow), Fraction II (gray), Fraction III (black) (Fig. 1, b). Centrifugation at 1300 g showed that the fractions have different specific gravity and settle as spatially differentiated sediments. The heaviest Fraction I is slightly darker than color of initial brass sample. We characterize the fractions with scanning electron microscopy (SEM), highlighting the change in powder's morphology. The brass particle surface in Fraction I is rough and contains etched areas that may indicate the occurrence of chemical reactions such as partial oxidation brass (Fig. 1f).

The XRD data of initial brass sample indicate the presence of two common brass types (Fig. 2**, plot 1**): *ca.* 91 % of α-phase (30 wt% of Zn

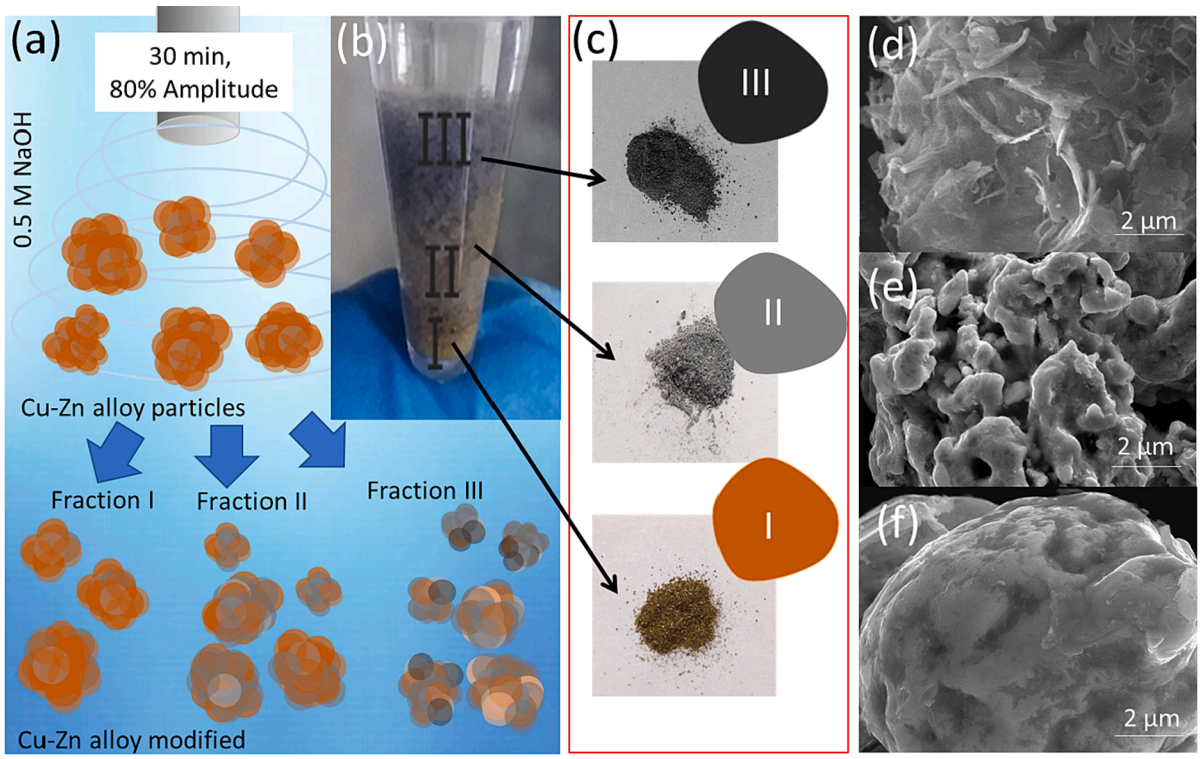

Fig. 1. A) the schematic illustration of ultrasound treatment of cu-zn alloy particles in 0.5 M NaOH during 30 min with 80 % of amplitude. After the sonochemical modification formed three fractions with different colors: Fraction I (yellow), Fraction II (gray), Fraction III (black) (b). c) The photos of the separated Fractions of Cu-Zn alloy. d–e) SEM images of Fraction III (d), Fraction II (e), and Fraction I (f).

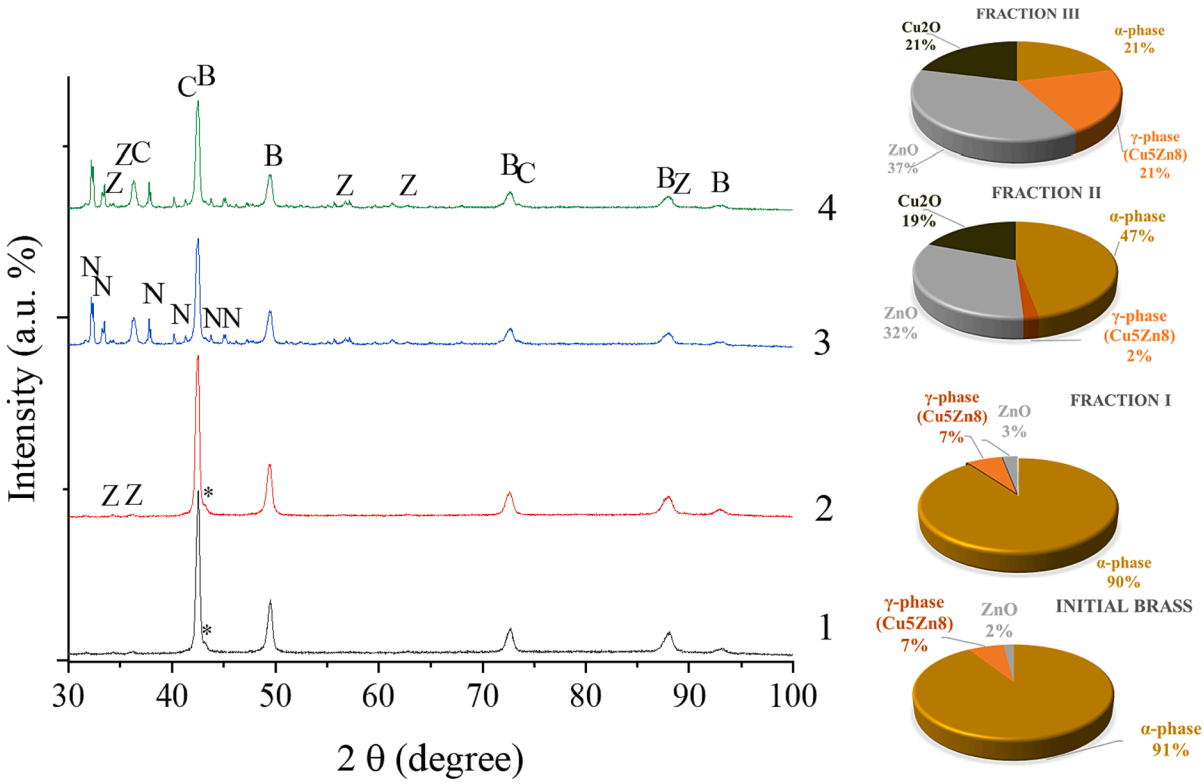

Fig. 2. XRD patterns of α-brass samples before (plot 1) and after sonochemical treatment at the intensity of 87 W/cm^2 for 30 min (plots 2–4). Fraction I is a plot 2, Fraction II is a plot 3, Fraction III is a plot 4. Abbreviations: B – α-brass, * – γ-brass (Cu_5Zn_8), N – $Na_2CO_3{\cdot}H_2O$, C –Cu_2O, Z – ZnO.

and 70 wt% of Cu) and *ca.* 7 % of Zn-rich γ-phase (Cu_5Zn_8). The rest 2 % is oxidized surface of brass particles. The computed crystallinity of the sample is *ca.* 65 %. The sonochemical treatment causes an obvious change in the computed crystallinity (68–75 %) of the samples compared to the pure brass powders (Fig. 1 c) that could also indicate the undergoing of chemical reactions. Preliminary results have shown that after sonication the brass for 1–3 min, the oxidized layer destroys and XRD pattern presented by α- brass and γ-brass. Further sonication initiates the zinc oxidation, and the ZnO content in Fraction 1 increases up to 3 wt%. The copper oxide phases in Fraction 1 were not detected (Fig. 2, plot 2).

To study the effect of temperature treatment, the brass samples were immersed in alkaline (0.5 M NaOH) and aqueous solutions (deionized water) for 30 min. The temperature of the aqueous solution was + 45 °C. The alkali solutions were kept at a temperature of + 20 °C and + 45 °C. The samples were kept for 30 min, then washed and dried in air at + 20 °C (**Figure S2 a**). It has been established that after processing a brass sample in distilled water at + 45 °C, *ca.* 99.5 wt% α-phase (30 wt% Zn and 70 wt% Cu) and 0.2 wt% (5 wt% Zn and 95 wt% Cu) and 0.3 wt% ZnO. While the original brass sample contains *ca.* 91 % α-phase (30 wt% Zn and 70 wt% Cu) and approx. 7 % zinc-rich γ-phase (Cu_5Zn_8). After treatment the brass sample in 0.5 M NaOH at + 25 °C, the content of the α-phase increases in the sample while the zinc oxide phase is absent. On increasing temperature treatment up to + 45 °C, the content of the brass phase enriched with copper increases to 0.7 wt% as well as 0.7 wt% of zinc oxide phase. It could be associated to the partial dissolution of zinc content in brass in an alkaline solution.

Since zinc is more chemically active than copper [23–26] we suggest that at first, during the brass oxidation transparent hydroxide and zinc oxide will be formed according to the reactions (Eqs. (1)–(2)):

$$2Zn + 2H_2O + O_2 \rightarrow 2Zn(OH)_2\downarrow \quad (1)$$

$$Zn(OH)_2 = ZnO + H_2O \qquad (100\text{–}250\ ^\circ C) \quad (2)$$

Despite the temperature in the volume of sonicated solution did not rise above + 45 °C, we have proposed some equations (Eqs. (2), 4, 7, 14, 17) of some phases formation at temperatures above 100 °C due to unique phenomena of collapsing cavitation bubble result in "hot-spot" generation. There are papers reported the experimentally measured values of temperature inside cavitation bubble in the range of ~5000 K depending on vapor pressure of the liquid that is being ultrasonicated [27,28].

K.S. Suslick [et al.] has shown that surfaces of sonicated particles can locally melt in the temperature range of 2600–3400 °C and form fused agglomerates of particles [29]. D.V. Andreeva [et al.] has studied which temperature is inside ultrasonically treated particles [30]. They have found that energy released from collapsed cavitation bubble can be controllably transferred to the sonication matter, and the particles can be heated up to average temperature of ~580 °C or even higher than *ca.* 1638 °C. That is why we have provided the reactions where some phase transformations could undergo due to the temperature effect. But this effect can exist only during the sonication, and we could not reach such temperatures in a solution without ultrasound.

In addition, sonochemical treatment may initiate Red-Ox processes [31,32], therefore, the following reactions could take place (Eq. (3) [10,25]):

$$Zn + 2OH^- - 2e^- = Zn(OH)_2\downarrow\ (E^0 = 1.25\ V) \quad (3)$$

In addition, in our previous articles [10,21,26] TEM microscopy clearly has shown the core–shell structure of the sonochemically modified zinc particles. The core of the particles was initial zinc whereas the shell was formed by a ZnO (1 0 1) phases.

Fraction 2 has a lower density, and yellow-grayish or light gray color, which may be due to the formation of copper oxides and hydroxides on the surface of the particles (Fig. 1 c). Fig. 1e shows the rough surface of the particles compared to the initial ones. The XRD measurement proves a partially oxidizing of copper in brass result in 9 wt% Cu_2O formation (Fig. 2, plot 3). The amount of ZnO increases up to 15 wt% whereas the content of the α- brass and γ-brass decreases to 22 wt% and 1 wt%, respectively. In addition, the sample contains a fraction of sodium hydroxide, which is formed during the sonochemical treatment and adsorbed on the particle surface. After thorough washing, it was found that the content of γ-brass and α-brass is 2 wt% and 47 wt%, respectively. The mass fraction of ZnO and Cu_2O increases to 32 wt% and 19 wt %, respectively. The formation of copper oxide can be explained according to the following reactions (Eqs. (4)–(7)):

$$4Cu + O_2 = 2Cu_2O\ (>200\ ^\circ C) \quad (4)$$

$$Cu_{(s)} + 2OH^-_{aq} - 2e^- = Cu_2O + H_2O\ (E^0 = 0.358\ V) \quad (5)$$

$$Cu_{(s)} + 2OH^-_{aq} - 2e^- = Cu(OH)_{2(s)}\ (E^0 = 0.224\ V) \quad (6)$$

$$Cu(OH)_{2(s)} + 2e^- = Cu_2O_{(s)} + 2OH^-_{aq} + H_2O\ (E^0 = -0.008\ V) \quad (7)$$

Reaction (4) (Eq. (4)) undergoes in absence of oxygen dissolved in an electrolyte. A decrease of the zinc-rich phase may occur due to the partial dissolution of zinc in alkaline solution according to the reactions (Eqs. (8)–(12)) described in [22,28]:

$$Zn + 2NaOH_{(conc)} + 2H_2O = Na_2[Zn(OH)_4] + H_2\uparrow \quad (8)$$

$$Zn(OH)_{2(s)} + 2NaOH_{(conc)} \leftrightarrow Na_2[Zn(OH)_4] \quad (9)$$

$$Zn + 4OH^- - 2e^- = ZnO_2^{2-} + 2H_2O\ (E^0 = 1.22\ V) \quad (10)$$

$$ZnO_{(s)} + 5\ H_2O \leftrightarrow [Zn(H_2O)_4]^{2+} + 2OH^- \quad (11)$$

$$Zn(OH)_{2(s)} + 4\ H_2O \leftrightarrow [Zn(H_2O)_4]^{2+} + 2OH^- \quad (12)$$

At the same time, these phases also may promote the reverse transformation of the soluable zinc fraction into zinc hydroxides and oxides (Eqs. (13)–(14)).

$$Na_2[Zn(OH)_4]_{(l)} = 2NaOH + Zn(OH)_2\downarrow \quad (13)$$

$$Na_2[Zn(OH)_4] \leftrightarrow ZnO_{(s)} + 2NaOH + H_2O\ (90\ ^\circ C) \quad (14)$$

The lightest Fraction 3 is dark grey (Fig. 1 c). The particles' surface is rough (Fig. 1 d). The X-ray analysis revealed the presence of 13 wt% copper (I) oxide, 3 wt% zinc oxide, 76 wt% α-brass and 8 wt% γ-brass. Zinc, as in Fraction 2, dissolves according to reactions (Eq. (8)–(12)). The decrease of the copper phase content and its oxides may be due to the reactions (Eqs. (15)–(17), [25]):

$$Cu_2O_{(s)} + H_2O \leftrightarrow 2Cu^+_{(l)} + 2OH^- \quad (15)$$

$$Cu_2O_{(s)} + 2NaOH_{(conc)} + H_2O \leftrightarrow 2Na[Cu(OH)_2] \quad (16)$$

$$Na[Cu(OH)_4]_{(l)} = CuO\downarrow + H_2O + 2NaOH\ (boiling) \quad (17)$$

Considering the above, we believe that ultrasound treatment does not affect the crystallite size of brass, but the change occurs locally on the surface of particles due to chemical reactions enhanced with cavitation.

In our previous work, we found that ultrasonic treatment helps to obtain materials capable to inhibit predominantly the growth of a particular strain. This phenomenon is associated with the prevalent release of copper or zinc ions [35]. In this research, we assume that Fractions I–III will release copper and zinc ions differently. To prove it, we applied the potentiometric titration method for all three fractions. (Fig. 3 **a-b**). The amount of released copper differs for three fractions with the maximum for Fraction III (30.591 μM), slightly less for Fraction II 28.111 (μM), and the heaviest Fraction I is the lowest by far. Extremely low thickness of modified layer obstructs accurate analysis of processes occurring on the surface since most methods provide information about objects of at least micrometer size. However, this limitation could be

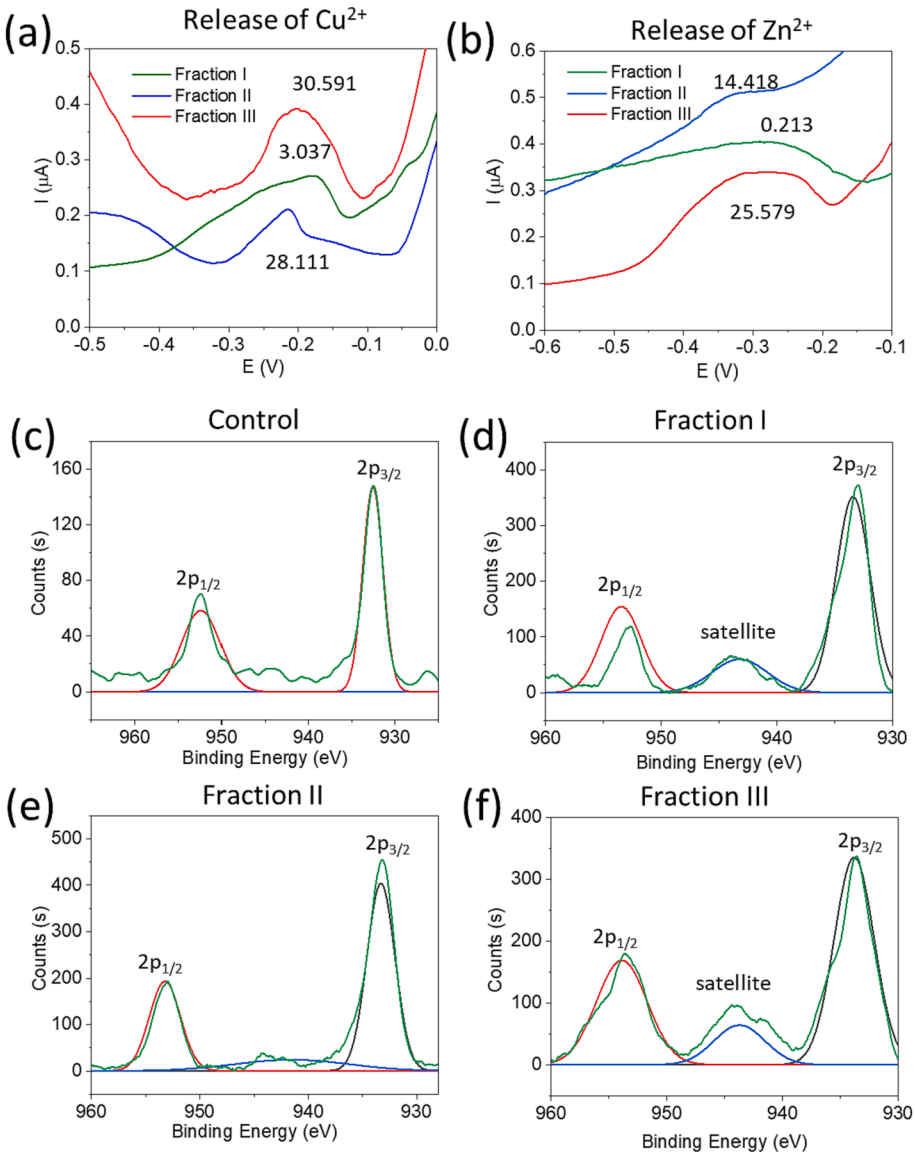

Fig. 3. Potentiometric titration for determining the release of copper ions (a) and zinc ions (b). Core-level XPS spectra of Cu 2p for control (c), Fraction I (d), Fraction II (e), Fraction III (f).

overcome with an X-ray photoelectron spectroscopy (XPS). The peaks at 1022.4 eV and 1045.4 eV confirm the presence of Zn^{2+} ions in Fraction I – III (not shown here). The peaks observed at 932.49 and 952.41 eV in the Cu 2p XPS spectrum of initial brass (Fig. 3 c–f) are attributed to Cu $2p^{3/2}$ and Cu $2p^{1/2}$, respectively. The satellite peaks in a range of 943–944 eV indicate the presence of Cu $^{+}$ and Cu^{2+} [36,37].

Despite the XRD analysis does not detect copper (II) phases in large quantities, XPS analysis proves the presence of Cu^{2+}. In particular, the characteristic satellite in Fig. 3 d corresponds to Cu^{2+} presence on the surface, but the release data shows negligible quantity. The Cu^{2+} and Zn^{2+} release is limited by a very low surface area of Cu-Zn particles. Depletion of Fraction I by zinc ions could be explained by simultaneous reactions (Eqs. (1)–(3)) and (Eqs. (4)–(6)) where zinc ions bonded in insoluble structures.

Interestingly, Fraction II has no satellite peaks characteristic of Cu^{2+}, while the copper peak is slightly shifted towards low binding energies (932.9 eV), which may be due to the presence of the copper (I) ions that corresponds to XRD analysis data [38]. At the same time, a large amount of Cu^{2+} is detected by titration. The formation of the Cu^{2+} could be explained by oxidation of Cu^{+} according to the reaction (Eq. (18)):

$$Cu^{+} + e^{-} = Cu^{2+}\ (E^{0} = -0.158\ V) \quad (18)$$

Thus, Fraction II predominantly release the Cu^{+} and Zn^{2+} ions whereas the copper (II) ions generation is delayed due to the reaction.

In Fraction III, the satellite peak corresponding to Cu^{2+} appears again. The peaks are shifted to 953.6 eV and 933.7 eV, that corresponds to the amorphous phase of CuO able to generate Cu^{2+} ions. In addition, the presence of Cu_2O could also promote the release of Cu^{+}. Besides, the release of Zn^{2+} is also observed.

Thus, we obtained three different copper and zinc-based materials via ultrasonic-assisted green synthesis. All the fractions are stable when exposed to air or water solutions and show no signs of degradation. However, Fraction III gains an outstanding copper release activity.

The intense collapse of cavitation bubbles creates significant local shock loads on particles [30,31]. Besides this effect, bubble explosion creates an ultrafast and ultra-strong thermal shock impact, an increase in temperature and pressure for a few μs at a localized area that also impact on particles [33]. It is known that all these influences can lead to a change in the phase structure, grain sizes, and various defects [7]. It can be controlled using the electron backscatter diffraction (EBSD)

method equipped with Field Emission Gun Scanning Electron Microscopes which can be applied for characterizing sub-micrometre grain structures [34].

In this paper, we assume that sonication could lead to the deformation of the malleable alloy and the accumulation of defects on the surface and in-depth. We use the EBSD method to study the defects that are energetically disadvantageous; therefore, dissolution and chemical transformation of defective structures are faster and easier. As a result, as seen in Fig. 4, the brass particle surface is activated, and various formation processes of oxides proceed very quickly on it, which acts as a source for the release of copper/zinc ions.

We compared biocide activity for five different bacterial strains, including gram-negative and gram-positive (Fig. 5). *Staphylococcus aureus* was chosen as an example of a Gram-positive strain whose suppression of development is of great importance for modern medicine. *Kebsiella pneumonae* is a gram-negative strain, however, unlike the gram-negative strains presented below, it forms capsules in the same way as *Staphylococcus aureus*. *Escherichia coli* has been used as an example of a classic Gram-negative strain, the suppression of which is also of great medical importance. In addition, *Pseudomonas aeruginosa* and *Enterobacter cloacae* are selected as Gram-negative strains. For the test, an amount of powder suspension was added into the bacterial culture in the Petri dish. The copper and zinc powders were used as the control samples.

Bacteria strains interacted differently with particle suspension. The histogram shows no inhibition zone after using initial brass suspension. The pure zinc particles promote the inhibition zones formation in the case of gram-positive staphylococcus bacteria, gram- negative *Escherichia coli* and *K. pneumoniae*. Whereas the other gram-negative strains are unsuppressed.

An area of inhibition zone correlates with the release activity of the Fractions. We suppose that the main contribution in biocide activity in Fraction I is caused by zinc ions due to the similar antibacterial behavior with zinc control. It should be mentioned that experimental data showed the predominant zinc ions release from γ-brass (Cu_5Zn_8), while initial brass sample releases almost no ions.

In addition to zinc ions, Fraction II generates mainly Cu^+, providing the possibility to study the sensitivity of the given strains to the combination of these ions (Fig. 5 k, l). The antibacterial activity of Fraction III is very similar to that of the copper control. Thus, we can conclude that the main contribution to the antibacterial properties is made by copper ions released from the surface of ultrasonically treated samples [35,36]. As Fraction III has the least amount of copper and zinc phases so we can assume the Fraction III to be the most biocidal.

To evaluate the influence of copper ions on bacteria the samples from inhibition zones were extracted and fixed for SEM studies (Fig. 5 f-j). The SEM images demonstrate a significant cell surface disruption compared to a normal state [37,38].

Copper ions are an important trace element in bacteria, but in excess, it is bacteriostatic. It is known that copper ions can be adsorbed on the surface of the cytoplasmic membrane, which has a negative charge. The ions then penetrate the bacteria and react with the sulfhydryl groups, causing the cells to die. In addition, Cu^{2+} can form free hydroxyl groups in the presence of oxygen, which destroy cell membranes [39–44]. Usually, Cu^{2+} has embedded in specific high-affinity sites in proteins or forms complexes with low molecular weight thiols (glutathione). Any excess Cu^{2+} that exceeds the binding rate may be incorrectly placed in non-specific and low-affinity metal ion binding sites. It could lead to the inactivation of important enzymes and disruption of normal metabolism [39,45]. The antibacterial properties of zinc ions are mainly associated with the generation of reactive oxygen species in oxygen or the formation of «zinc fingers» [40–46]. Interestingly, brass samples treated in aqueous and alkaline solutions at room and high temperatures without ultrasound do not demonstrate the biocidal effect unlike Fractions (I–III)

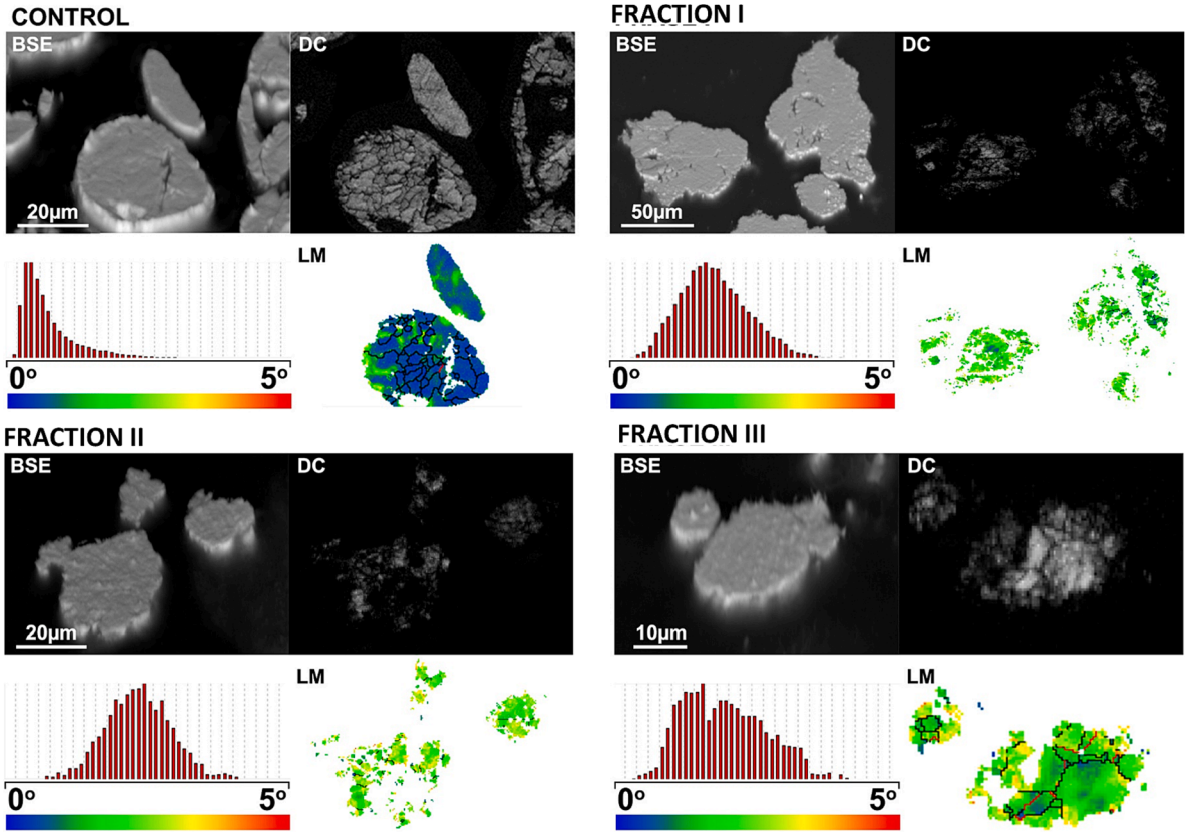

Fig. 4. Electron backscatter diffraction studies of initial (control) and ultrasonically treated CuZn particles. All the studied samples are represented as images in backscattered electrons (BSE), diffraction contrast (DC) and local misorientation (LM) images. Legends and distribution graphs correspond to LM images.

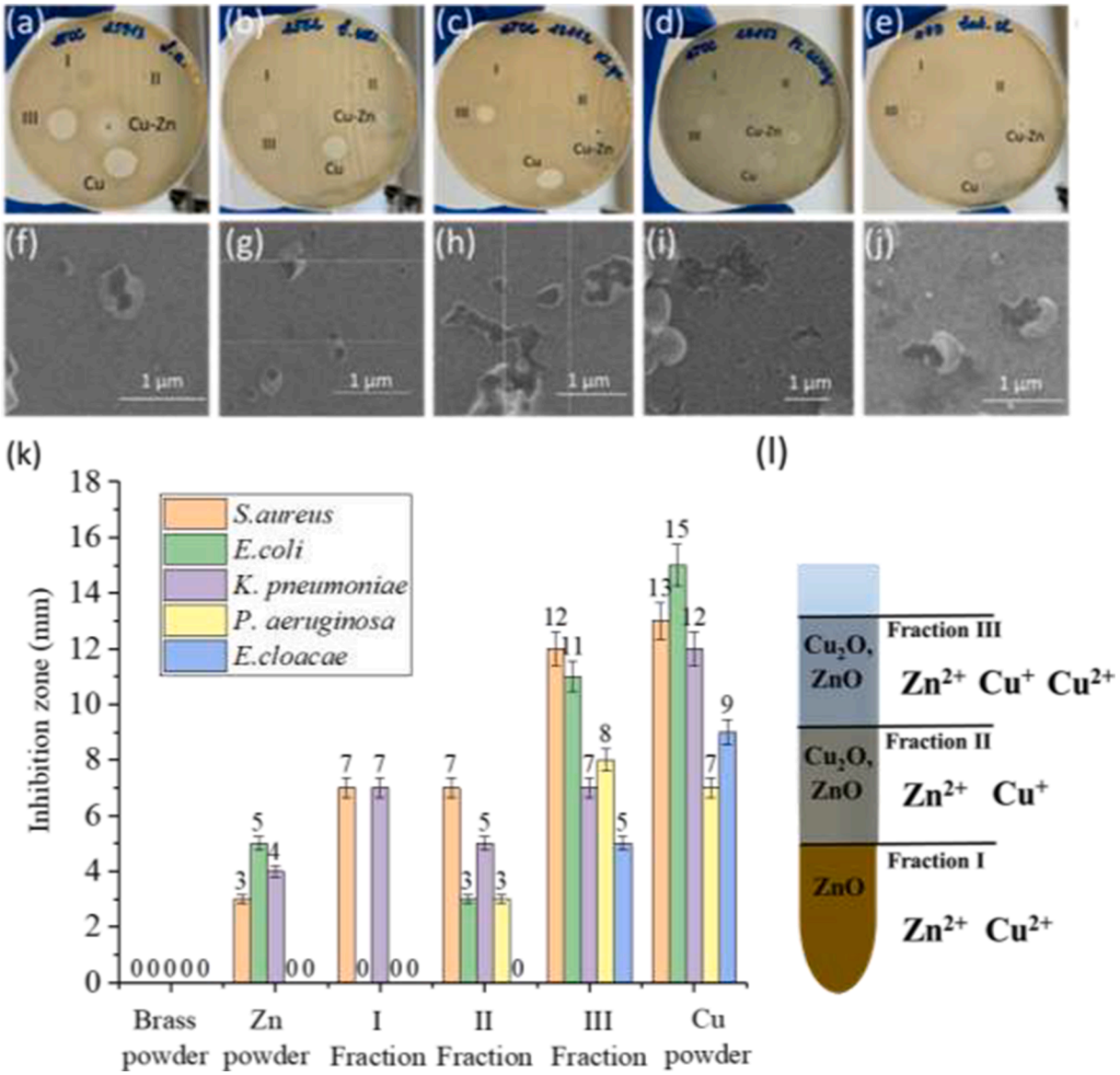

Fig. 5. A-e) the photo of inhibition zone diameter of three fractions and cu powder for*S. aureus, E. coli, K. pneumoniae, P. aeruginosa, and E. cloacae*, respectively. f) - j) Scanning electron microscopy images of bacterial cell damage. k) Ratio of inhibition zone for five bacterial strains and powders of brass, copper and zinc particles taken as controls. Error bars are s.d. values, $p < 0.05$. (l) The scheme of the predominant ions release from Fractions I-III.

do (Table S1, Supporting materials). It may be due to the ability of ultrasound to accelerate the undergoing of Red-Ox reactions followed by formation of oxide and hydroxide phases on the surface that are capable of releasing zinc and copper cations, which have various toxic effect on bacteria.

4. Conclusions

We have successfully fabricated gradient materials by sonication of Cu-Zn alloy. After the sonication, the alloy is easily separated at three different fractions possessing different surface morphology and release activity of copper ions.

The high-energy treatment of a brass powder in a basic medium allows a soft modification of the particle's surface. Sonication leads to a fast formation of slightly soluble phases without great effect on the particle's inner structure and mechanical properties. The materials are stable both exposed to air or in water solutions and exhibit outstanding antibacterial properties. Both potentiometric titration and XPS show the presence of mobile Cu^{+}, Cu^{2+} and Zn^{2+}. The amount of released copper ions correlates with the area of inhibition zone in biocide properties tests which allows us to attribute antibacterial activity to Cu^{+}, Cu^{2+} release. SEM studies confirm the hypothesis showing highly disrupted bacteria. The disruption might be caused by the bacteria membrane damage caused by copper and zinc ions.

CRediT authorship contribution statement

Mirna Sabbouh: Investigation. **Anna Nikitina:** Data curation, Writing – original draft. **Elizaveta Rogacheva:** Investigation. **Anna Nebalueva:** Resources. **Vladimir Shilovskikh:** Data curation, Validation, Methodology. **Roman Sadovnichii:** Validation, Methodology. **Aleksandra Koroleva:** Validation. **Konstantin Nikolaev:** Conceptualization, Methodology. **Lyudmila Kraeva:** Conceptualization, Methodology, Supervision. **Sviatlana Ulasevich:** Conceptualization, Writing – review & editing, Supervision, Funding acquisition. **Ekaterina Skorb:** Conceptualization, Methodology, Supervision.

Declaration of Competing Interest

The authors declare that they have no known competing financial interests or personal relationships that could have appeared to influence the work reported in this paper.

Acknowledgments

Authors acknowledge RSF grant no. 19-79-10244. Priority 2030 Federal Academic Leadership Program is acknowledged for infrastructural support. The XPS studies were performed at the «Physical Methods of Surface Investigation» center, SEM EDX and EBSD studies were performed at "Geomodel" center at Saint-Petersburg State University.

Appendix A. Supplementary data

Supplementary data to this article can be found online at https://doi.org/10.1016/j.ultsonch.2022.106247.

References

[1] G. Canavese, A. Ancona, L. Racca, M. Canta, B. Dumontel, F. Barbaresco, T. Limongi, V. Cauda, Nanoparticle-assisted ultrasound: A special focus on sonodynamic therapy against cancer, Chem. Eng. J. 340 (2018) 155–172, https://doi.org/10.1016/j.cej.2018.01.060.
[2] Z. Gao, H. Zhu, X. Li, P. Zhang, M. Ashokkumar, F. Cavalieri, J. Hao, J. Cui, Sono-Polymerization of Poly(ethylene glycol)-Based Nanoparticles for Targeted Drug Delivery, ACS Macro Lett. 8 (2019) 1285–1290, https://doi.org/10.1021/acsmacrolett.9b00576.
[3] L.H. Thompson, L.K. Doraiswamy, Sonochemistry: Science and engineering, Ind. Eng. Chem. Res. 38 (1999) 1215–1249, https://doi.org/10.1021/ie9804172.
[4] S.K. Gujar, P.R. Gogate, Application of hybrid oxidative processes based on cavitation for the treatment of commercial dye industry effluents, Ultrason. Sonochem. 75 (2021), https://doi.org/10.1016/j.ultsonch.2021.105586.
[5] M. Bradley, M. Ashokkumar, F. Grieser, Sonochemical production of fluorescent and phosphorescent latex particles, J. Am. Chem. Soc. 125 (2003) 525–529, https://doi.org/10.1021/ja0268581.
[6] P.V. Cherepanov, M. Ashokkumar, D.V. Andreeva, Ultrasound assisted formation of Al-Ni electrocatalyst for hydrogen evolution, Ultrason. Sonochem. 23 (2015) 142–147, https://doi.org/10.1016/j.ultsonch.2014.10.012.
[7] P.V. Cherepanov, D.V. Andreeva, P.V. Cherepanov, D.V. Andreeva, Phase structuring in metal alloys: Ultrasound-assisted top-down approach to engineering of nanostructured catalytic materials, Ultrason. Sonochem. 35 (2017) 556–562, https://doi.org/10.1016/j.ultsonch.2016.05.006.
[8] B.G. Pollet, The use of ultrasound for the fabrication of fuel cell materials, Int. J. Hydrogen Energy 35 (2010) 11986–12004, https://doi.org/10.1016/j.ijhydene.2010.08.021.
[9] J. Theerthagiri, J. Madhavan, S.J. Lee, M.Y. Choi, M. Ashokkumar, B.G. Pollet, Sonoelectrochemistry for energy and environmental applications, Ultrason. Sonochem. 63 (2020), 104960, https://doi.org/10.1016/j.ultsonch.2020.104960.
[10] S.A. Ulasevich, E.I. Koshel, I.S. Kassirov, N. Brezhneva, L. Shkodenko, E.V. Skorb, Oscillating of physicochemical and biological properties of metal particles on their sonochemical treatment, Mater. Sci. Eng. C 109 (2020), 110458, https://doi.org/10.1016/j.msec.2019.110458.
[11] M. Kamali, M. Davarazar, T.M. Aminabhavi, Single precursor sonochemical synthesis of mesoporous hexagonal-shape zero-valent copper for effective nitrate reduction, Chem. Eng. J. 384 (2020), 123359, https://doi.org/10.1016/j.cej.2019.123359.
[12] G. Chatel, How sonochemistry contributes to green chemistry? Ultrason. Sonochem. 40 (2018) 117–122, https://doi.org/10.1016/j.ultsonch.2017.03.029.
[13] N. Pazos-Perez, T. Borke, D.V. Andreeva, R.A. Alvarez-Puebla, Silver coated aluminium microrods as highly colloidal stable SERS platforms, Nanoscale 3 (2011) 3265–3268, https://doi.org/10.1039/c1nr10403a.
[14] B. Lindström, L.J. Pettersson, G. Menon, Activity and characterization of Cu/Zn, Cu/Cr and Cu/Zr on γ-alumina for methanol reforming for fuel cell vehicles, Appl. Catal. A 234 (2002) 111–125, https://doi.org/10.1016/S0926-860X(02)00202-8.
[15] H.Y. Chen, S.P. Lau, L. Chen, J. Lin, C.H.A. Huan, K.L. Tan, J.S. Pan, Synergism between Cu and Zn sites in Cu/Zn catalysts for methanol synthesis, Appl. Surf. Sci. 152 (1999) 193–199, https://doi.org/10.1016/S0169-4332(99)00317-7.
[16] L. Alejo, R. Lago, M.A. Peña, J.L.G. Fierro, Partial oxidation of methanol to produce hydrogen over Cu-Zn-based catalysts, Appl. Catal. A 162 (1997) 281–297, https://doi.org/10.1016/S0926-860X(97)00112-9.
[17] E. Dauvergne, C. Lacquemant, C. Adjidé, C. Mullié, Validation of a worst-case scenario method adapted to the healthcare environment for testing the antibacterial effect of brass surfaces and implementation on hospital antibiotic-resistant strains, Antibiotics 9 (5) (2020) 245.
[18] R. Quezada, Y. Quintero, J.C. Salgado, H. Estay, A. García, Understanding the phenomenon of copper ions release from copper-modified TFC membranes: A mathematical and experimental methodology using shrinking core model, Nanomaterials 10 (2020) 1–18, https://doi.org/10.3390/nano10061130.
[19] W. Dröge, Free radicals in the physiological control of cell function, Physiol. Rev. 82 (2002) 47–95, https://doi.org/10.1152/physrev.00018.2001.
[20] X. Jin, I.H. Riedel-Kruse, Biofilm Lithography enables high-resolution cell patterning via optogenetic adhesin expression, PNAS 115 (2018) 3698–3703, https://doi.org/10.1073/pnas.1720676115.
[21] J. Gensel, T. Borke, N.P. Pérez, A. Fery, D.V. Andreeva, E. Betthausen, A.H. E. Müller, H. Möhwald, E.V. Skorb, Cavitation engineered 3D sponge networks and their application in active surface construction, Adv. Mater. 24 (2012) 985–989, https://doi.org/10.1002/adma.201103786.
[22] M. Sabbouh, A. Nikitina, E. Rogacheva, L. Kraeva, S.A. Ulasevich, E.V. Skorb, M. Nosonovsky, Separation of motions and vibrational separation of fractions for biocide brass, Ultrason. Sonochem. 80 (2021), 105817, https://doi.org/10.1016/j.ultsonch.2021.105817.
[23] S.V. Gudkov, D.E. Burmistrov, D.A. Serov, M.B. Rebezov, A.A. Semenova, A. B. Lisitsyn, A mini review of antibacterial properties of ZnO nanoparticles, Front. Phys. 9 (2021), 641481, https://doi.org/10.3389/fphy.2021.641481.
[24] R.A. Lidin et al., Chemical properties of inorganic substances: Textbook for universities (Moscow, Khimiya, 2000) (ISBN 5-7245-1163-0).
[25] P.W. Atkins, Physical Chemistry, 6th ed., Freeman, W.H, 1997.
[26] L. Saunders, Surface and Colloid Chemistry, 1951. https://doi.org/10.1111/j.2042-7158.1951.tb13130.x.
[27] J. Rae, M. Ashokkumar, O. Eulaerts, C. von Sonntag, J. Reisse, F. Grieser, Estimation of ultrasound induced cavitation bubble temperatures in aqueous solutions Ultrason, Sonochem. 12 (2005) 325–329, https://doi.org/10.1016/j.ultsonch.2004.06.007.
[28] V. Misik, N. Miyoshi, P., Riesz EPR spin-trapping study of the sonolysis of H_2O/D_2O mixtures: probing the temperatures of cavitation regions, J. Phys. Chem. 99 (1995) 3605–3611, https://doi.org/10.1021/j100011a030.
[29] S.J. Doktycz, K.S. Suslick, Interparticle Collisions Driven by Ultrasound, Science 247 (4946) (1990) 1067–1069, https://doi.org/10.1126/science.2309118.
[30] P.V. Cherepanov, A. Kollath, D.V. Andreeva, Up to which temperature ultrasound can heat the particle? Ultrason. Sonochem. 26 (2015) 9–14, https://doi.org/10.1016/j.ultsonch.2015.03.002.
[31] E.V. Skorb, H. Möhwald, Ultrasonic approach for surface nanostructuring, Ultrason. Sonochem. 29 (2016) 589–603, https://doi.org/10.1016/j.ultsonch.2015.09.003.
[32] J. Dulle, S. Nemeth, E.V. Skorb, D.V. Andreeva, Sononanostructuring of zinc-based materials, RSC Adv. 2 (2012) 12460–12465, https://doi.org/10.1039/c2ra22200k.
[33] D.V. Andreeva, P.V. Cherepanov, Y.S. Avadhut, J. Senker, Rapidly oscillating microbubbles force development of micro-and mesoporous interfaces and composition gradients in solids, Ultrason. Sonochem. 51 (2019) 439–443, https://doi.org/10.1016/j.ultsonch.2018.07.024.
[34] F.J. Humphreys, Characterisation of fine-scale microstructures by electron backscatter diffraction (EBSD), Scr. Mater. 51 (8) (2004) 771–776, https://doi.org/10.1016/j.scriptamat.2004.05.016.
[35] M. Zhukov, M.S. Hasan, P. Nesterov, M. Sabbouh, O. Burdulenko, E.V. Skorb, M. Nosonovsky, Topological Data Analysis of Nanoscale Roughness in Brass Samples, ACS Appl. Mater. Interfaces 14 (2022) 2351–2359, https://doi.org/10.1021/acsami.1c20694.
[36] E. Kaprara, P. Seridou, V. Tsiamili, M. Mitrakas, G. Vourlias, I. Tsiaoussis, G. Kaimakamis, E. Pavlidou, N. Andritsos, K. Simeonidis, Cu-Zn powders as potential Cr(VI) adsorbents for drinking water, J. Hazard. Mater. 262 (2013) 606–613, https://doi.org/10.1016/j.jhazmat.2013.09.039.
[37] C. Berne, E. Andrieu, J. Reby, J.-M. Sobrino, C. Blanc, Dissolution Kinetics of α, β′-Brass in Basic NaNO 3 Solutions, J. Electrochem. Soc. 163 (2016) C7–C15, https://doi.org/10.1149/2.0071602jes.
[38] J. Morales, J.P. Espinos, A. Caballero, A.R. Gonzalez-Elipe, J.A. Mejias, XPS study of interface and ligand effects in supported Cu2O and CuO nanometric particles, J. Phys. Chem. B 109 (2005) 7758–7765, https://doi.org/10.1021/jp0453055.
[39] X. Dou, Y. Chen, H. Shi, $CuBi_2O_4$/BiOBr composites promoted PMS activation for the degradation of tetracycline: S-scheme mechanism boosted Cu^{2+}/Cu^{+} cycle, Chem. Eng. J. 431 (2022), 134054, https://doi.org/10.1016/j.cej.2021.134054.
[40] F. Chen, X. Zhao, H. Liu, J. Qu, Reaction of $Cu(CN)_{32}$- with H_2O_2 in water under alkaline conditions: Cyanide oxidation, Cu^{+}/Cu^{2+} catalysis and H_2O_2 decomposition, Appl. Catal. B Environ. 158–159 (2014) 85–90, https://doi.org/10.1016/j.apcatb.2014.04.010.
[41] G. Sánchez-Sanhueza, B.-T. Fuentes-Rodríguez, Helia, Copper Nanoparticles as Potential Antimicrobial Agent in Disinfecting Root Canals. A Systematic Review. Nanopartículas de Cobre como Potencial Agente Antimicrobiano en la Desinfección de Canales Radiculares, Revisión Sistemática, Int. J. Odontostomat. Int. J. Odontostomat. 10 (2016) 547–554. https://scielo.conicyt.cl/pdf/ijodontos/v10n3/art24.pdf.
[42] N. Cioffi, M. Rai, Nano-antimicrobials: Progress and prospects, 2012. https://doi.org/10.1007/978-3-642-24428-5.
[43] R. Xue, Y. Liu, Q. Zhang, C. Liang, H. Qin, P. Liu, K.e. Wang, X. Zhang, L.i. Chen, Y. Wei, R.M. Kelly, Shape changes and interaction mechanism of Escherichia coli cells treated with sericin and use of a sericin-based hydrogel for wound healing, Appl. Environ. Microbiol. 82 (15) (2016) 4663–4672.
[44] D.J. Hess, M.J. Henry-Stanley, A.M.T. Barnes, G.M. Dunny, C.L. Wells, Ultrastructure of a Novel Bacterial Form Located in Staphylococcus aureus In Vitro

and In Vivo Catheter-Associated Biofilms, J. Histochem. Cytochem. 60 (2012) 770–776, https://doi.org/10.1369/0022155412457573.
[45] K.Y. Djoko, M.M. Goytia, P.S. Donnelly, M.A. Schembri, W.M. Shafer, A. G. McEwan, Copper(II)-bis(thiosemicarbazonato) complexes as antibacterial agents: Insights into their mode of action and potential as therapeutics, Antimicrob. Agents Chemother. 59 (2015) 6444–6453, https://doi.org/10.1128/AAC.01289-15.
[46] E. Zhang, X. Zhao, J. Hu, R. Wang, S. Fu, G. Qin, Antibacterial metals and alloys for potential biomedical implants, Bioact. Mater. 6 (2021) 2569–2612, https://doi.org/10.1016/j.bioactmat.2021.01.030.